



**HAL**  
open science

## Direct Synthesis of Mesoionic Carbene (MIC)-Stabilized Gold Nanoparticles from 1,2,3-Triazolium Salts

Alexandre Porcheron, Omar Sadek, Salem Ba Sowid, Nathalie Bridonneau, Laura Hippolyte, Dimitri Mercier, Philippe Marcus, Lukmonjon Mutalliev, Clément Chauvier, Corinne Chanéac, et al.

► **To cite this version:**

Alexandre Porcheron, Omar Sadek, Salem Ba Sowid, Nathalie Bridonneau, Laura Hippolyte, et al.. Direct Synthesis of Mesoionic Carbene (MIC)-Stabilized Gold Nanoparticles from 1,2,3-Triazolium Salts. *Chemistry of Materials*, 2023, 35 (17), pp.6865-6876. 10.1021/acs.chemmater.3c01162 . hal-04185135v2

**HAL Id: hal-04185135**

**<https://hal.science/hal-04185135v2>**

Submitted on 22 Aug 2023

**HAL** is a multi-disciplinary open access archive for the deposit and dissemination of scientific research documents, whether they are published or not. The documents may come from teaching and research institutions in France or abroad, or from public or private research centers.

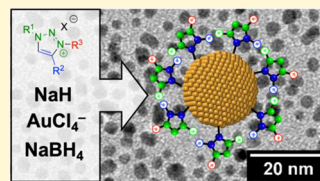
L'archive ouverte pluridisciplinaire **HAL**, est destinée au dépôt et à la diffusion de documents scientifiques de niveau recherche, publiés ou non, émanant des établissements d'enseignement et de recherche français ou étrangers, des laboratoires publics ou privés.

# Direct Synthesis of Mesoionic Carbene (MIC)-Stabilized Gold Nanoparticles from 1,2,3-Triazolium Salts

Published as part of the *Chemistry of Materials virtual special issue "In Honor of Prof. Clement Sanchez"*.

Alexandre Porcheron, Omar Sadek, Salem Ba Sowid, Nathalie Bridonneau, Laura Hippolyte, Dimitri Mercier, Philippe Marcus, Lukmonjon Mutalliev, Clément Chauvier, Corinne Chanéac, Louis Fensterbank,\* and François Ribot\*

**ABSTRACT:** Significant achievements have been reported in the last few years regarding the stabilization and functionalization of gold nanoparticles (AuNPs), mainly through the use of thiols and imidazolylidene N-heterocyclic carbene-capping ligands. Herein, we report that mesoionic carbene (MIC) ligands, based on the 1,2,3-triazol-5-ylidene scaffold, allow the expeditive preparation of AuNPs of very high stability through a simple and straightforward one-pot protocol directly from triazolium salts and separated Au(III) sources. Control over the size of AuNPs has been achieved by varying the Au/ligand ratio as well as the nature of the triazolium salts, the latter being facilitated by the ease of synthesis of the MIC precursors through click chemistry. Characterization of these MIC-AuNPs by  $^{13}\text{C}$  solid-state (ss) NMR and X-ray photoelectron spectroscopy (XPS) hints at the exclusive presence of MICs on the surface of nanoparticles solely comprising Au(0).



## 1. INTRODUCTION

Nanoparticles are one of the main pillars on which nanotechnologies have been flourishing over the last decades. The significant surface-to-mass ratio and peculiar properties that matter can exhibit at such a scale constitute the central motivations of academic and industrial interest in nanoparticles.<sup>1</sup> Gold nanoparticles (AuNPs), due to their plasmonic properties and various applications, are one of the most studied systems.<sup>2</sup> They form a fertile ground for the design of novel applications in the fields of medicine, biosensors, or catalysis.<sup>3</sup> In this context, expanding the toolbox available to synthesize stable AuNPs, with the control of size and properties, is a topic of intense research interest.

AuNPs require surface ligands to kinetically protect them from irreversible aggregation, in addition to providing the desired functionalization for targeted applications. Over the last decade, N-heterocyclic carbenes (NHCs) have emerged as a promising family of surface ligands.<sup>4</sup> These ligands, which possess a formally divalent carbon atom, are able to form strong covalent bonds with surface metal atoms. For example, (benz)imidazolium-based NHCs were shown to be excellent ligands for the functionalization of gold surfaces.<sup>5</sup> Cyclic (alkyl)(amino)carbenes (CAACs) were also recently successfully deposited on gold surfaces.<sup>6</sup>

NHCs based on the 1,3-imidazol-2-ylidene scaffold (ImNHC)<sup>7</sup> have received significant attention, mainly owing to the stability they impart to surfaces and to their relative ease of preparation and handling.<sup>4</sup> Stable ImNHC-decorated AuNPs were seminally prepared by ligand exchange in a top-

down approach by Chechik and co-workers,<sup>8</sup> while Vignolle and Tilley<sup>9</sup> employed a bottom-up approach by reducing ImNHC-Au(I) halide complexes (Figure 1). Capitalizing on these studies, many groups have studied the synthesis and properties of NHC-stabilized AuNPs,<sup>10</sup> which often display

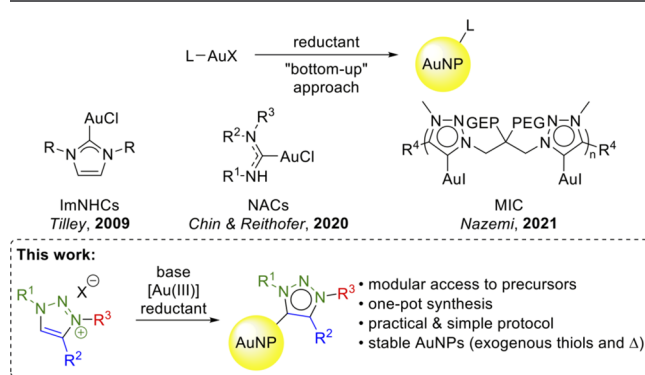


**Figure 1.** NHC-, NAC-, and MIC-Au(I) complexes for NHC-, NAC-, and MIC-AuNP synthesis (top) and the synthesis and stabilization of MIC-AuNPs from triazolium salts (bottom, this work).

Received: May 15, 2023

Revised: July 27, 2023

high colloidal stability even under harsh conditions (acidic and basic media, high and low temperatures, and salinity), a point of paramount importance in many applications. Nevertheless, these ImNHC platforms are not ideal when non-C2 symmetrical or multifunctional species are desired, requiring tedious multistep syntheses.

Recently, Reithofer and co-workers introduced nitrogen acyclic carbenes (NACs) (Figure 1) in an effort to increase the diversity of carbenic ligands able to stabilize AuNPs.<sup>11</sup> NAC-ligated AuNPs stable to thiol exchange were obtained, though the need to handle isocyanide derivatives somewhat limits the possibility of diversification.

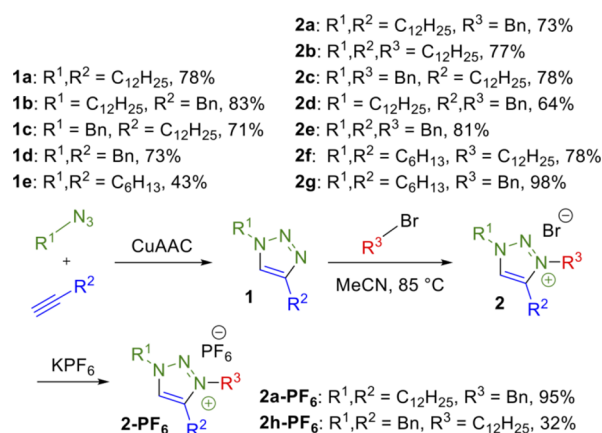
Alternatively, mesoionic carbenes (MICs), based on the 1,2,3-triazol-5-ylidene scaffold, offer excellent modularity and facile access to a diverse pool of potential ligands. Their preparation relies on the highly versatile copper-catalyzed alkyne-azide click (CuAAC) reaction,<sup>12</sup> and the quaternarization of  $\gamma$ -nitrogen ( $N^3$ ), thereby allowing the introduction of up to three distinct substituents on the MIC core. Moreover, MICs are known to be stronger  $\sigma$ -donors than ImNHCs,<sup>13</sup> which should result in a stronger coordination to the surface atoms. The potentiality of MICs in the field of metallic nanoparticles and surfaces was actually mentioned by Bertrand and co-workers<sup>14</sup> but remained unexplored until recently.<sup>15</sup> At the end of 2021, Nazemi and co-workers reported on MIC-stabilized AuNPs that were prepared from a polymeric or a monomeric MIC-Au(I) iodide complex.<sup>15a</sup> The chosen MIC platform incorporated oligoethylene oxide chains, rendering the obtained AuNPs water-soluble. While the polymeric MIC-Au(I) complex required a multistep synthesis, the resulting AuNPs were highly stable under various conditions, including the presence of exogenous thiols (Figure 1). The high stability was attributed to the multidentate nature of the polymeric MIC surface ligand. This is supported by the lower stability of the nanoparticles obtained from the monomeric MIC-Au(I) iodide complex. Even more recently, Guo and co-workers compared the MIC-stabilized AuNPs obtained from MIC-Au(I) chloride complexes with those derived from triazolium tetrachloroaurate.<sup>15b</sup> Both approaches concluded that two long alkyl chains (i.e., dodecyl,  $C_{12}H_{25}$ ) are required on the MIC core to yield stable AuNPs. They also observed that the Au(0)/Au(I) ratio and the size of the AuNPs depended on the synthesis protocol used.

Building on our long-standing interest and sustained research activity in the synthesis of MIC-stabilized gold nanoparticles (MIC-AuNPs),<sup>16</sup> we herein report an alternative and simpler synthesis, which directly uses 1,2,3-triazolium salts and tetrachloroauric acid to prepare MIC-AuNPs (Figure 1). The procedure is very straightforward, as it does not require the preparation nor the isolation of any MIC-Au(I)-X or triazolium-AuCl<sub>4</sub> complexes. It also allows the facile modulation of the ligand-to-gold ratio, a parameter known to influence the AuNP size.<sup>17</sup> A library of triazolium salts was tested to possibly evidence the influence of the lateral chains and the nature of the anion.

## 2. RESULTS AND DISCUSSION

**2.1. Synthesis of Triazolium Salt Precursors.** Our synthesis began with a click CuAAC reaction to provide the corresponding 1,2,3-triazoles **1** in moderate to good yields (Scheme 1). Given the importance of the steric character in NHC-stabilized AuNPs, alkynes and azides of various substitutions were chosen to provide triazoles with long

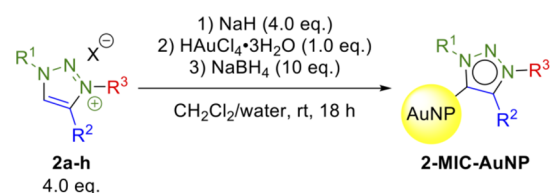
### Scheme 1. Synthesis of 1,2,3-Triazolium Salts **2** from 1,2,3-Triazoles **1** (Bn = Benzyl)



( $C_{12}H_{25}$ ), short ( $C_6H_{13}$ ), and mixed (benzyl) lateral chains. This would allow us to evaluate the effect and limits of such MIC ligands on the stabilization of the derived AuNPs. With these derivatives in hand, facile quaternization of  $N^3$  with an alkyl bromide in MeCN at 85 °C provided the corresponding triazolium bromide salts **2** in good to excellent yields. Anion metathesis was performed on **2a** to provide the triazolium hexafluorophosphate **2a-PF<sub>6</sub>** to investigate the effect of the counterion on nanoparticle synthesis. This was also applied to synthesize **2h-PF<sub>6</sub>**, as the bromide salt **2h** could not be obtained in pure form.

**2.2. Synthesis of MIC-AuNPs.** Seeking to develop a versatile and streamlined platform for the synthesis of MIC-AuNPs, we designed and optimized our protocol to allow the direct reduction of a gold precursor in the presence of triazolium salt MIC precursors (Scheme 2). This methodology

### Scheme 2. Synthesis of 2-MIC-AuNPs



presents several advantages. First, this avoids the requirement to synthesize, isolate, and purify the corresponding MIC-Au(I) halide or triazolium-AuCl<sub>4</sub> complexes. Second, the Au/ligand ratio is not limited to 1:1 and can be easily varied. This opens the possibility to tune the size of the MIC-AuNPs, as we have previously demonstrated with NHC-AuNPs.<sup>17</sup>

Practically, the protocol is relatively straightforward: the triazolium precursor **2** is premixed with NaH, followed by the addition of the Au(III) precursor prior to the addition of NaBH<sub>4</sub> as the reducing agent. Addition of NaBH<sub>4</sub> causes a color change from clear yellow/orange to dark burgundy/red, which is highly indicative of gold reduction and AuNP formation. Following reaction workup, MIC-AuNPs are precipitated from CH<sub>2</sub>Cl<sub>2</sub> with ethanol and collected by centrifugation. This purification process comprising two precipitation cycles is important to remove any traces of molecular species that could remain. The obtained MIC-AuNPs were characterized by UV/vis spectroscopy, TEM, and, for selected examples, by <sup>13</sup>C ssNMR and XPS.

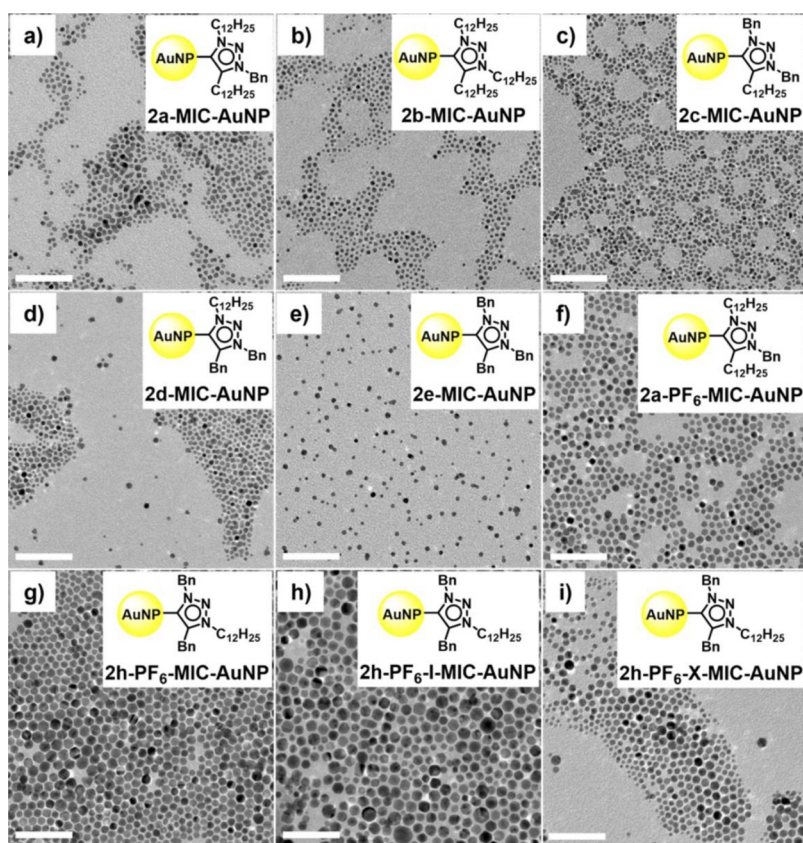


Figure 2. TEM images of 2-MIC-AuNPs. Scale bar: 50 nm.

Table 1. Average Particle Sizes and Plasmon Resonance Band (PRB) Maxima for the Synthesized MIC-AuNPs

entry	MIC-AuNP	size $\pm$ SD (nm) <sup>a</sup>	PI (%) <sup>b</sup>	PRB $\lambda_{\max}$ (nm) <sup>c</sup>
1	2a-MIC-AuNP	3.2 $\pm$ 0.6	19	522
2	2a-I-MIC-AuNP <sup>d</sup>	4.3 $\pm$ 1.1	26	524
3	2a-PF <sub>6</sub> -MIC-AuNP	5.1 $\pm$ 0.8	16	524
4	2a-PF <sub>6</sub> -I-MIC-AuNP <sup>d</sup>	5.2 $\pm$ 1.5	29	519
5	2b-MIC-AuNP	3.0 $\pm$ 0.6	20	517
6	2c-MIC-AuNP	2.8 $\pm$ 0.5	18	523
7	2d-MIC-AuNP	3.2 $\pm$ 0.8	25	524
8	2e-MIC-AuNP	3.2 $\pm$ 0.8	25	524
9	2h-PF <sub>6</sub> -MIC-AuNP	7.4 $\pm$ 1.8	24	523
10	2h-PF <sub>6</sub> -I-MIC-AuNP <sup>d</sup>	8.8 $\pm$ 2.5	28	523
11	2h-PF <sub>6</sub> -X-MIC-AuNP <sup>e</sup>	4.7 $\pm$ 1.6	34	521

<sup>a</sup>Determined by TEM, SD: standard deviation. <sup>b</sup>Polydispersity index (PDI) corresponds to the ratio of the standard deviation to the average size. <sup>c</sup>UV/vis spectra collected using CH<sub>2</sub>Cl<sub>2</sub> solutions. <sup>d</sup>Using 1.0 equivalent of the corresponding triazolium salt 2. <sup>e</sup>Using 10 equivalents of the corresponding triazolium salt 2.

Almost all triazolium salts **2** allowed the isolation of spherical MIC-AuNPs that proved stable for months in suspension in CH<sub>2</sub>Cl<sub>2</sub> (Figure 2 and Table 1). All isolated MIC-AuNPs displayed a plasmon resonance band (PRB) in the UV/vis spectrum in the range of 517–529 nm (Table 1). As expected, the long alkyl chains (C<sub>12</sub>H<sub>25</sub>) at the lateral positions (N<sup>1</sup> and C<sup>4</sup>) of **2a** and **2b** allowed the synthesis and isolation of stable and spheroidal AuNPs of 3.2  $\pm$  0.6 and 3.0  $\pm$  0.6 nm for **2a-MIC-AuNP** and **2b-MIC-AuNP**, respectively (Figure 2a,b). ‘Unsymmetrically’ substituted triazolium salts **2c** and **2d**, with lateral benzyl and dodecyl substituents, also allow the isolation of stable MIC-AuNPs of 2.8  $\pm$  0.5 and 3.2  $\pm$  0.8 nm for **2c-MIC-AuNP** and **2d-MIC-AuNP**, respectively (Figure 2c,d). Intriguingly, triazolium salt **2e**, which possesses

only flanking benzyl substituents, also allowed the isolation of stable MIC-AuNPs of 3.2  $\pm$  0.8 nm for **2e-MIC-AuNPs** (Figure 2e). This suggests that long-chain alkyl substituents are not crucial for the preservation of AuNP integrity, provided that benzyl substituents are present in the vicinity of the carbenic center. In contrast, while triazolium salts **2f** and **2g**, with short C<sub>6</sub>H<sub>13</sub> alkyl chains on N<sup>1</sup> and C<sup>4</sup>, did allow the formation of AuNPs, as observed by the formation of a dark red solution during the reaction, stable AuNPs could not be isolated, as they irreversibly precipitated during the purification process. Similar issues for NP stabilization have been observed when using ImNHCs with too short lateral chains.<sup>10a</sup> However, contrary to Guo’s observations,<sup>15b</sup> a single dodecyl lateral chain appears to provide enough stabilization, when combined

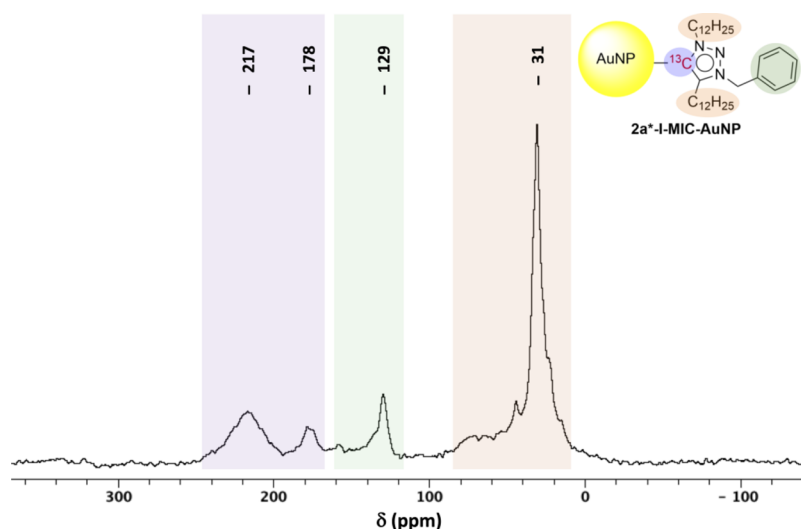


**Figure 3.**  $^{13}\text{C}$  CP/MAS NMR spectrum of  $2\text{a}^*\text{-I-MIC-AuNP}$ . The peaks at 217 and 178 ppm (purple shaded area) are attributed to  $^{13}\text{C}$ -Au environments on nanoparticles. The peaks at 129 ppm (green shaded area) and 31 ppm (orange shaded area) are attributed to the aromatic and aliphatic carbon atoms, respectively.

with benzyl groups on the MIC core. Remarkably, a MIC bearing only benzyl substituents can efficiently stabilize AuNPs. For all the triazolium bromide salts used, which yield stable nanoparticles ( $2\text{a}$  to  $2\text{e}$ ), sizes around 3 nm (with a polydispersity index of 20–25%) are obtained when 4 equiv triazolium is introduced in the synthesis.

Interestingly, when triazolium  $2\text{a}$  was associated with a  $\text{PF}_6^-$  counterion instead of  $\text{Br}^-$ , the nanoparticles obtained were almost 2 nm larger, as the  $2\text{a-PF}_6\text{-MIC-AuNP}$  sample was found to be  $5.1 \pm 0.8$  nm in size as observed by TEM (Figure 2f). This counterion effect seems even more pronounced with triazolium salts decorated with benzyl groups on  $\text{N}^1$  and  $\text{C}^4$ . Indeed,  $2\text{h-PF}_6$  provided  $2\text{h-PF}_6\text{-MIC-AuNP}$ , with a size of  $7.4 \pm 1.8$  nm, while  $2\text{e-MIC-AuNP}$  exhibits a size of only  $3.2 \pm 0.8$  nm (Figure 2e,g).

**2.3. Tuning of MIC-AuNP Size.** The majority of isolated MIC-AuNPs displayed very similar sizes, ranging from 2.8 to 3.2 nm (Table 1). However,  $2\text{a-PF}_6\text{-MIC-AuNP}$  and  $2\text{h-PF}_6\text{-MIC-AuNP}$  demonstrate that the AuNP size can be modified by the nature of the triazolium salt and its counterion ( $5.1 \pm 0.8$  and  $7.4 \pm 1.8$  nm, Table 1, entries 3 and 9, respectively).

To further investigate the tunability and control of nanoparticle size, we varied the ratio of Au(III) and triazolium salt precursors. Starting with the triazolium salts  $2\text{a}$  and  $2\text{a-PF}_6$ , no significant difference in MIC-AuNP sizes was observed by increasing the Au/triazolium salt ratio to 1:1 (compared to the 1:4 ratio described above).  $2\text{a-I-MIC-AuNP}$  and  $2\text{a-PF}_6\text{-I-MIC-AuNP}$  exhibit sizes of  $4.3 \pm 1.1$  and  $5.2 \pm 1.5$  nm, respectively (Figures S2 and S8), as compared to  $2\text{a-MIC-AuNP}$  and  $2\text{a-PF}_6\text{-MIC-AuNP}$ , with sizes of  $3.2 \pm 0.6$  nm and  $5.1 \pm 0.8$  nm, respectively (Figure 2a,g). However, modifying the Au/triazolium salt ratio with the precursor  $2\text{h-PF}_6$  allowed for the control of the AuNP size. Increasing the Au/ $2\text{h-PF}_6$  ratio to 1:1 allowed the isolation of  $2\text{h-PF}_6\text{-I-MIC-AuNP}$  with a larger size of  $8.8 \pm 2.5$  nm, while decreasing the ratio to 1:10 allowed the isolation of  $2\text{h-PF}_6\text{-X-MIC-AuNP}$  with a smaller size of  $4.7 \pm 1.6$  nm, as observed by TEM (Table 1, entries 10 and 11, and Figure 2h,i; also see Figures S9–S11).

Together, these findings highlight the modularity of access to various ligands that can be used to stabilize AuNPs. These

MIC precursors demonstrate the flexibility, and limitations, of varying lateral ( $\text{N}^1$  and  $\text{C}^4$ ) and backbone ( $\text{N}^3$ ) substituents of differing steric character for the synthesis and isolation of stable MIC-AuNPs. Notably, the size of MIC-AuNPs can be controlled by the nature of the triazolium salt precursor as well as the Au/triazolium ratio. This size modulation likely results from a subtle equilibrium between the availability of the surface ligands, which stabilize the NP, and the kinetics of reduction, which controls the number of nuclei. On one side, the more triazolium salts are introduced, the more MICs are generated and the smaller the NPs are. On the other side, the triazolium counterion ( $\text{Br}^-$  vs  $\text{PF}_6^-$ ) by interacting with Au(III) can change its redox potential.<sup>18</sup>

**2.4. NMR Spectroscopy Studies.** Solution-state  $^1\text{H}$  NMR spectroscopy performed on purified MIC-AuNP suspensions did not allow us to conclude on the nature of capping ligands (see Figures S24 and S25). Indeed, ligands grafted on nanoparticles are usually quite silent, especially the sites which lie the closest to the surface and, accordingly, bear the information on grafting. This feature is related to the distribution of local environments and the strong shortening of the transverse relaxation time, which is related to a decrease of the local mobility.<sup>9,17,19</sup> Both effects are responsible for the broadening of the signals, which finally disappear into the baseline. In conclusion, the only information that solution-state  $^1\text{H}$  NMR brought was that our suspensions of purified MIC-AuNPs did not contain any residual molecular species.

To circumvent these limitations of solution NMR spectroscopy for the study of NPs,  $^{13}\text{C}$  solid-state NMR (ss NMR) was preferred to gain insights into the coordination of the MIC ligand on the surface. We first synthesized MIC-AuNPs using the pro-carbenic  $^{13}\text{C}$ -labeled version of ligand  $2\text{a}$  ( $2\text{a}^*$ ), according to the normal protocol, using 1 equiv  $2\text{a}^*$  relative to Au(III), to give  $2\text{a}^*\text{-I-MIC-AuNP}$  after purification. Solution NMR spectroscopic analysis of  $2\text{a}^*\text{-I-MIC-AuNP}$  confirmed again the absence of molecular species in the  $^1\text{H}$  and especially the  $^{13}\text{C}$  spectra (see Figures S26 and S27).<sup>20</sup> The solid-state  $^{13}\text{C}$  CP/MAS (cross-polarization magic angle spinning) NMR spectrum obtained for  $2\text{a}^*\text{-I-MIC-AuNP}$  is presented in Figure 3. By comparison with the data reported for

NHC<sup>5a,21</sup> and CAAC<sup>22</sup> carbenes coordinated to Au(0), the signals at 216 and 178 ppm have been attributed to the <sup>13</sup>C-labeled carbenic carbon coordinated to the NP surface. The presence of two signals for the carbenic carbon in **2a**\*-I-MIC-AuNP is likely related to the existence of different types of coordination geometries and/or exposed surfaces. A similar observation has already been reported for NHC-stabilized ruthenium nanoparticles<sup>19a</sup> and predicted by DFT calculations for NHC attached to Cu(100) or Cu(111) surfaces.<sup>23</sup> The other signals observed at 129 and 31 ppm can be easily attributed to the aromatic and aliphatic carbons of the MIC ligand, respectively. Though not enriched, these carbons are easily observed as they correspond to several atoms, yield narrower resonances, and benefit more strongly from the cross-polarization, as they are close to one or more hydrogen atoms. In line with this interpretation, the <sup>13</sup>C CP/MAS NMR spectrum of **2a**-I-MIC-AuNP also displays the resonances at 129 and 31 ppm but is void of any signals at 217 and 178 ppm (Figure S32).

**2.5. XPS Studies.** To gain further insights into the surface structure of these nanoparticles, XPS analyses were carried out on starting triazolium salts **2a**, **2h**-PF<sub>6</sub>, and their corresponding MIC-AuNPs. Regarding the starting triazolium salts, the analysis of each relevant photopeak (C 1s, N 1s, Br 3d, F 1s, and P 2p) confirmed the expected stoichiometry for each precursor (see Figures 4, S14, S15, and Table S1 for complete

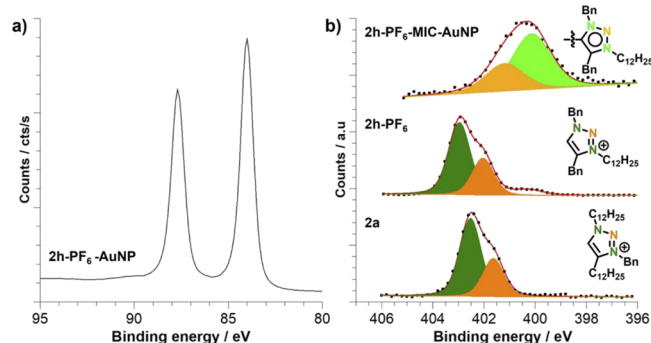


**Figure 4.** XPS spectra of (a) Au 4f for **2h**-PF<sub>6</sub>-MIC-AuNP and (b) N 1s for **2h**-PF<sub>6</sub>-MIC-AuNP (top), **2h**-PF<sub>6</sub> (middle), and **2a** (bottom).

details, including the stability of samples under X-ray irradiation (Figure S16).<sup>24</sup> The analysis of the N 1s photopeaks for **2a** and **2h**-PF<sub>6</sub> clearly reveals two components (in a 2:1 ratio), ca. 403 and 402 eV, separated by the same energy shift of 0.9 eV (Figure 4). The weak energy-binding shift (~0.4 eV) observed between **2a** and **2h**-PF<sub>6</sub> might be due to the chemical substituents carried by the triazolium core (two C<sub>12</sub>H<sub>25</sub> and one benzyl for **2a** vs two benzyls and one C<sub>12</sub>H<sub>25</sub> for **2h**-PF<sub>6</sub>) or to the anion. The presence of two N 1s components can be correlated to the presence of two types of N atoms with different environments: the external atoms (R<sup>1</sup>-N=N-R<sup>2</sup>) and the central one (R<sup>1</sup>-N=N-R<sup>2</sup>). According to the intensity ratio and the positive charge, which is carried by the external nitrogen atoms, the component at high binding energy (~403 eV) can be attributed to the two outer  $\alpha$ -N<sup>1</sup> and  $\gamma$ -N<sup>3</sup> atoms, while the component at low binding energy (~402 eV) can be attributed to the central  $\beta$ -N<sup>2</sup> atom of the triazolium salt.

The analysis of **2h**-PF<sub>6</sub>-MIC-AuNP showed the presence of carbon, nitrogen, and gold, the characteristic of the AuNP. No

phosphorus nor fluorine, which would indicate the presence of PF<sub>6</sub><sup>-</sup> residue, was detected. The Au 4f spectrum (Figure 4) shows two peaks at 84.0 and 87.6 eV (Au 4f<sub>7/2</sub> and Au 4f<sub>5/2</sub>, respectively) that are characteristic of spin-orbit splitting and confirm that the nanoparticles are exclusively composed of Au(0), with no traces of Au(I) or remaining Au(III) precursor. This feature makes our MIC-AuNPs clearly different from those reported by Nazemi and co-workers<sup>15a</sup> or Guo and co-workers,<sup>15b</sup> which, according to XPS, also contain various amounts of Au(I). The analysis of the N 1s spectrum confirms the absence of the starting triazolium salt **2h**-PF<sub>6</sub> as its main photopeaks (~403 eV) are absent. Accordingly, XPS strongly supports that the surface is exclusively covered by MIC ligands. Further analysis of the N 1s photopeak revealed two distinct components at 401.2 and 400.2 eV in a 1:2 ratio. As for the triazolium starting salt, the two N 1s components can likely be linked to the two types of nitrogen environments present in the MIC ligand. The low-intensity component (401.2 eV) is attributed to the central  $\beta$ -N<sup>2</sup> atom, and the more intense component (~400.2 eV) is assigned to both the  $\alpha$ -N<sup>1</sup> and  $\gamma$ -N<sup>3</sup> atoms in the triazolylidene cycle (Figure 4).

The attribution we proposed for the N 1s photopeaks is coherent with the changes that take place between the ligand precursor, i.e., the triazolium, and the MIC ligand. Indeed, upon deprotonation of a triazolium to form an MIC, there is a global loss of charge in the heterocycle. Moreover, this loss should be mostly experienced by the external N atoms, which previously carried the positive charge (i.e.,  $\alpha$ -N<sup>1</sup> and  $\gamma$ -N<sup>3</sup>). Accordingly, the binding energy of these external N atoms is the one that most significantly changes ( $\Delta E_b = -2.7$  eV), while the binding energy of the central  $\beta$ -N<sup>2</sup> is practically unaffected. Such a decrease of the N 1s binding energy, in relation with a loss of charge, has already been described when comparing an imidazolium salt to its corresponding ImNHC-AuNP ( $\Delta E_b = -1.4$  eV).<sup>17</sup>

**2.6. Stability Studies.** The thermal and chemical stability of AuNPs is an important aspect for these materials depending on their targeted application. In this context, **2a**-MIC-AuNP was evaluated as a model material. The stability of the samples was studied by monitoring any changes in the PRB by UV/vis spectroscopy that are indicative of AuNP aggregation (red shift, decrease in peak intensity, and peak broadening). Gold nanoparticles from **2a**-MIC-AuNP were found to be relatively stable to a high concentration of exogenous thiol (10 mM dodecanethiol in CH<sub>2</sub>Cl<sub>2</sub>) over several days (Figure 5a). After an initial 5% decrease in peak intensity after 5 min of exposure, decreases in peak intensity were marginal with only 10 and 14% decrease after 24 h and 5 days, respectively. Importantly, only changes in peak intensity are observed without the red shift of the PRB maximum or ripening. TEM analysis of nanoparticles after 24 h in the thiol solution shows that they maintain their spherical shape and present an identical size to the starting material (3.3 ± 0.6 nm; see Figure S19). As a complement to these studies, a sample at 24 h time-point was also analyzed by XPS. The characteristic signals of **2a**-MIC-AuNP were observed (C 1s, N 1s, and Au 4f). Yet, an additional weak doublet at 162.0 and 163.2 eV was also observed (see Figure S20), indicating the presence of sulfur bound to gold.<sup>25</sup> However, due to the inconsistency in the expected peak area ratio (theoretically S 2p<sub>1/2</sub>/S 2p<sub>3/2</sub> = 0.5), free thiol is also likely present (binding energy 163.6 and 164.9 eV for S 2p<sub>3/2</sub> and S 2p<sub>1/2</sub>, respectively). The amount of free thiol can be estimated to account for around 25% of the total

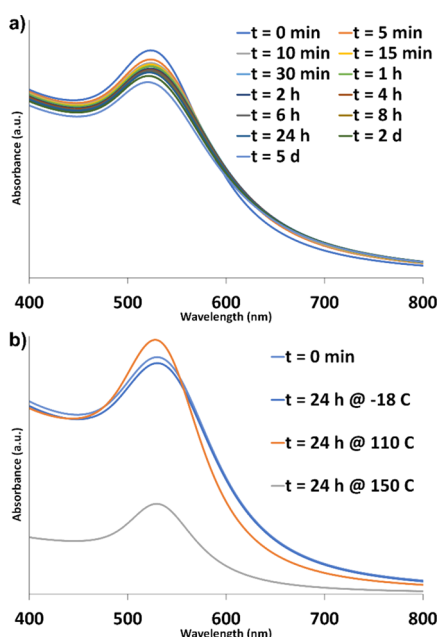


**Figure 5.** UV/vis spectra of (a) **2a-MIC-AuNP** in 10 mM dodecanethiol in  $\text{CH}_2\text{Cl}_2$  and (b) **2a-MIC-AuNP** in toluene at various temperatures.

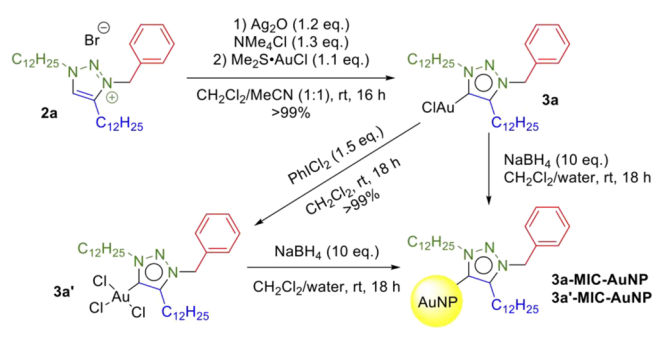
measured sulfur. Due to the overall low amount of sulfur detected by XPS ( $\text{S } 2p/\text{N } 1s = 0.13$ ), it is difficult to conclude whether a low substitution of MIC by sulfur has occurred or this is simply the adsorption of traces of DDT on the “non-occupied” surface sites. The stability observed by UV/vis and TEM studies would seem to support the latter. Importantly, the stability observed with these new materials and the fact that thiols may coordinate onto the “non-occupied” sites on the MIC-AuNP surface are highly interesting as they open a path toward the synthesis of tailored materials with different types of surface ligands.

Thermal stability was evaluated by dispersing **2a-MIC-AuNP** in toluene and exposing the solution to various conditions. The nanoparticles showed high thermal stability, with almost no degradation observed after 24 h at  $-18^\circ\text{C}$  (Figure 5b). Additionally, heating the same sample at  $110^\circ\text{C}$  for 24 h only resulted in the PRB band slightly sharpening with no loss in intensity or significant shift in its  $\lambda_{\text{max}}$  (Figure 5b). TEM analysis shows almost no evolution of the average size ( $3.8 \pm 1.4$  nm; see Figure S22); however, a few larger AuNPs can be observed. Heating the same sample to  $150^\circ\text{C}$  for 24 h causes a significant degradation, evidenced by a large decrease in peak intensity. Moreover, TEM analysis shows that the remaining AuNPs have doubled their average size ( $6.4 \pm 1.8$  nm; see Figure S23).

These results demonstrate that MIC-AuNPs exhibit very good stability to exogenous thiols, comparable to that of bidentate NHC-stabilized AuNPs.<sup>26</sup> Such a property has also been reported by Nazemi and co-workers, with AuNPs stabilized by polymeric MIC ligands in water.<sup>15a</sup>

**2.7. Comments on Reaction Paths.** To probe if our MIC-AuNP syntheses could include the in situ formation of MIC-Au complexes, we synthesized MIC-Au(I)Cl (**3a**) and MIC-Au(III)Cl<sub>3</sub> (**3a'**) from triazolium bromide **2a** following known protocols (Scheme 3).<sup>27</sup> The isolated complexes **3a** and **3a'** were then subjected to the same NP synthetic protocol, in the absence of now redundant NaH, used for **2-MIC-AuNP**.

**Scheme 3. Synthesis of MIC-Au(I) and Au(III) Chloride Complexes **3a** and **3a'** and the Corresponding **3a/3a'-MIC-AuNP****



Intriguingly, under otherwise identical conditions, the reduction step and consequent formation of NPs using molecular Au(I) and Au(III) chloride complexes, **3a** and **3a'**, appeared significantly slower than that in our one-pot method with triazolium bromide **2a** (10–15 min vs instantaneous, respectively). This kinetic difference was qualitatively observed by the time taken for the reaction mixture to turn deep burgundy red, a color indicating the formation of MIC-AuNPs.

The isolated nanoparticles, **3a-MIC-AuNP**, presented a slightly red-shifted PRB at 536 nm compared to **2a-I-MIC-AuNP** (524 nm). The TEM analysis of **3a-MIC-AuNP** showed that spherical nanoparticles are obtained with a size of  $5.0 \pm 1.2$  nm (see Figure S12), which is similar to the size of **2a-I-MIC-AuNP** ( $4.3 \pm 1.1$  nm). However, **3a'-MIC-AuNP** presented an even more red-shifted PRB at 549 nm, with a slightly bigger size of  $5.9 \pm 0.9$  nm (see Figure S13). Both suspensions, **3a-MIC-AuNP** and **3a'-MIC-AuNP** in  $\text{CH}_2\text{Cl}_2$ , were stable for months. These findings confirm that MIC-Au(I) complexes are viable precursors for MIC-AuNPs<sup>15</sup> and also demonstrate that MIC-Au(III) complexes can be used. However, the difference in reaction kinetics observed between our one-pot process and the reduction of molecular complexes suggests that different mechanisms are most likely at play. The direct synthesis reported here with triazolium salts and  $\text{HAuCl}_4$  does not seem to involve an in situ-generated MIC-Au(III)Cl<sub>3</sub> complex.

**2.8. Catalytic Activity of MIC-AuNP in the Reduction of 4-Nitrophenol.** The potential catalytic applications of MIC-AuNPs were explored in the reduction of 4-nitrophenol (4-NP) into 4-aminophenol (4-AP) using  $\text{NaBH}_4$  as the reductant. This model reaction has been extensively studied as a benchmark to investigate the AuNP catalytic activity.<sup>4a,15a,28</sup> Indeed, the 4-NP concentration can be conveniently monitored during the course of the reaction via UV/vis spectroscopy. This reaction is usually performed in water and therefore requires AuNPs that can be dispersed in water.<sup>15a</sup> However, reports have also shown that it can proceed in biphasic systems (e.g.,  $\text{H}_2\text{O}/\text{CH}_2\text{Cl}_2$ ), with the reagents in the aqueous phase and the AuNP catalyst in the organic phase.<sup>29</sup> Interestingly, this biphasic system offers the advantage of easily removing the catalyst at the end of the reaction through a convenient separation of the organic and aqueous phases.

Mixing 4-NP with an excess of  $\text{NaBH}_4$  in water resulted in the formation of a bright yellow solution of 4-nitrophenolate anions, which exhibit a characteristic absorption peak at 400 nm (Figure 6a). No further evolution of the UV/vis spectrum occurred until the addition, under vigorous stirring, of the

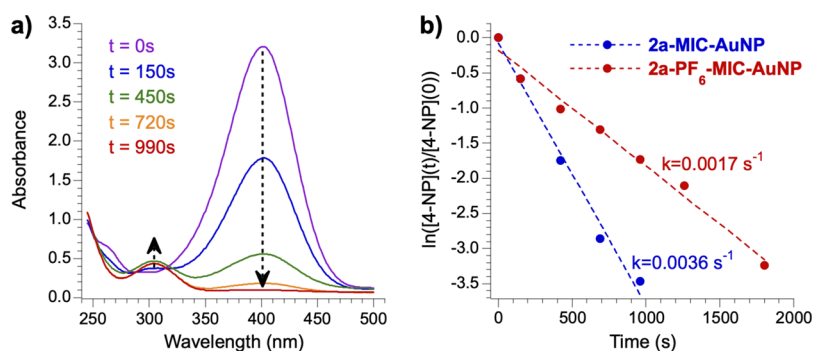


**Figure 6.** Catalytic activity of MIC-AuNPs. (a) UV/vis spectra of the aqueous phase at different times during the reduction of 4-nitrophenol (4-NP) into 4-aminophenol (4-AP) by  $\text{NaBH}_4$  in the presence of **2a-MIC-AuNP**. (b) Monitoring of the 4-NP concentration with time in the presence of **2a-MIC-AuNP** (blue) or **2a-PF<sub>6</sub>-MIC-AuNP** (red).

MIC-AuNPs dispersed in  $\text{CH}_2\text{Cl}_2$ . Then, the color of the aqueous phase gradually changed from bright yellow to colorless within several minutes. This color change arises from the decrease of the 400 nm absorption ( $A_{400}$ ), associated to a lowering of the 4-NP concentration, and the growth of an absorption peak at 300 nm, in line with the increase of the 4-aminophenolate concentration.<sup>29b</sup> The plot of  $\ln([4\text{-NP}](t)/[4\text{-NP}](0))$ , which is equal to  $\ln(A_{400}(t)/A_{400}(0))$ , vs time indicated a pseudo-first-order kinetic model (Figure 6b) and allowed us to estimate the reaction rate constant ( $k$ ). A value of  $0.0036 \text{ s}^{-1}$  was found for **2a-MIC-AuNP**. It is comparable to previous reports obtained in biphasic systems.<sup>29b</sup>

The influence of the MIC-AuNP size and surface ligand on their catalytic properties was also investigated. Compared to **2a-MIC-AuNP**, **2a-PF<sub>6</sub>-MIC-AuNP** (Figure 6b), which displays the same surface ligand but has a larger size ( $5.1 \pm 0.8 \text{ nm}$  vs  $3.2 \pm 0.6 \text{ nm}$ ), gave a lower  $k$  value ( $0.0017 \text{ s}^{-1}$ ) for the same loading (0.02 mg). This difference can be attributed to the lower total surface area developed by the same mass of the larger NP. The rate constants obtained for **2b-MIC-AuNP** and **2e-MIC-AuNP** (Figure S33), which exhibit similar sizes to **2a-MIC-AuNP** ( $3.0 \pm 0.6$  and  $3.2 \pm 0.8 \text{ nm}$ , respectively, vs  $3.2 \pm 0.6 \text{ nm}$ ), but MIC surface ligands with different side groups, are reported in Table 2. To correct for the differences in

**Table 2. Summary of the MIC-AuNP Catalysis Results**

catalyst	mass of catalyst (mg)	$k$ ( $\text{s}^{-1}$ )	$k_{\text{nor}}$ ( $\text{s}^{-1} \text{ mg}^{-1}$ )
<b>2a-MIC-AuNP</b>	0.02	0.0036	0.18
<b>2a-PF<sub>6</sub>-MIC-AuNP</b>	0.02	0.0017	0.09
<b>2b-MIC-AuNP</b>	0.02	0.0018	0.09
<b>2e-MIC-AuNP</b>	0.012	0.0028	0.23

catalyst loadings, the rate constants were normalized according to the mass of the catalyst used. The obtained normalized rate constants ( $k_{\text{nor}} = k/\text{mass}$ ) ranged from  $0.09 \text{ s}^{-1} \text{ mg}^{-1}$  for **2b-MIC-AuNP** to  $0.23 \text{ s}^{-1} \text{ mg}^{-1}$  for **2e-MIC-AuNP**, with an intermediate value,  $0.18 \text{ s}^{-1} \text{ mg}^{-1}$ , for **2a-MIC-AuNP**. These differences in activity might be related to the accessibility of the substrate (4-NP) to the NP surface. Long alkyl chains ( $\text{C}_{12}\text{H}_{25}$ ) would create a more hydrophobic surface detrimental to 4-NP access, while comparatively smaller benzyl groups would favor this access.

The MIC-AuNPs prepared in this work demonstrated catalytic activities in the reduction of 4-NP comparable to those previously reported for other AuNPs in biphasic systems.<sup>29b</sup> Moreover, their activity appears to be controlled

and governed by the side groups of the MIC surface ligands, thereby demonstrating further that surface modification can alter the chemical properties of the nano-objects.

### 3. CONCLUSIONS

The use of 1,2,3-triazolium salts, as platforms for MIC ligand precursors, allows the synthesis and stabilization of gold nanoparticles, as exemplified in this work. Rich structural diversity of ligands is easily attainable by leveraging the modularity of the CuAAC reaction. Additionally, the procedure for nanoparticle synthesis is simple, involving a one-pot protocol from triazolium salt to MIC-AuNPs under mild conditions. In contrast to previous protocols,<sup>15</sup> this method obviates the need to prepare and purify MIC-Au(I) or triazolium- $\text{AuCl}_4$  complexes. Moreover, this method yields MIC-AuNPs made only of Au(0). This approach works with a series of triazolium salts to give stable MIC-AuNPs whose size can be changed from 3 to 9 nm with the nature of the ligand and the Au/ligand ratio. Such size variation for MIC-AuNPs is reported here for the first time.

These MIC-AuNPs exhibit a high colloidal stability against exogenous thiols and harsh thermal conditions. Their precise formation mechanism remains to be unraveled, but it likely does not involve the in situ formation of MIC-Au(I) or MIC-Au(III) complexes, as, if both species can also yield MIC-AuNPs, they do so more slowly. These MIC-AuNPs also exhibit catalytic activity in the reduction of 4-nitrophenol to 4-aminophenol.

Owing to the rich and simple functionalization chemistry that triazoliums provide with their three substituents on the heterocycle, and the high colloidal stability of MIC-AuNPs, they will likely allow the development of diverse applications that would be difficult with thiols or ImNHC-stabilized AuNPs.

### 4. EXPERIMENTAL SECTION

**4.1. Materials and Methods.** All reactions were performed in oven-dried glassware under air or an argon atmosphere as stated. Dry solvents were obtained as follows: (1)  $\text{CH}_2\text{Cl}_2$  was dried over  $\text{CaH}_2$  and collected by distillation; (2) MeCN was dried under argon over activated 3 Å molecular sieves. Other solvents used were of commercial grade and used as received with no drying unless otherwise noted. All chemicals were purchased from commercial sources and used as received unless otherwise stated. Deuterated solvents for NMR spectroscopic analysis were purchased from Eurisotop.

NMR experiments were performed in deuterated solvents.  $^1\text{H}$ ,  $^{13}\text{C}$ ,  $^{19}\text{F}$ , and  $^{31}\text{P}$  NMR spectra were recorded on Avance 300 MHz,



Avance 400 MHz, or Avance 600 MHz Bruker spectrometers. All spectra were recorded at ambient temperature (300 K). Chemical shifts ( $\delta$ ) are reported in parts per million (ppm) relative to the residual protium in the solvents ( $^1\text{H}$ ) or the solvent signal ( $^{13}\text{C}$ ) as internal standards. External  $\text{H}_3\text{PO}_4$  (85%) in water and  $\text{CFCl}_3$  were used as references for  $^{31}\text{P}$  and  $^{19}\text{F}$  NMR, respectively. Multiplicity of signals is indicated using the following abbreviations: s (singlet), b (broad), d (doublet), dd (doublet of doublet), t (triplet), q (quadruplet), p (pentet), hept (heptet), and m (multiplet).

Solid-state  $^{13}\text{C}$  NMR spectra were recorded under cross-polarization (CP) magic-angle spinning (MAS) conditions on a Bruker Avance III 500 spectrometer, operating at 500.50 and 125.85 MHz for  $^1\text{H}$  and  $^{13}\text{C}$ , respectively. The sample was packed in a 4 mm  $\text{ZrO}_2$  rotor and spun at 14 kHz. A contact time of 2 ms and a recovery delay of 2 s were used for the cross-polarization. 112,640 transients (63 h) were summed. MIC-AuNPs, loaded onto KBr, were packed into the  $\text{ZrO}_2$  rotor. To maximize detection sensitivity, solid KBr was used as the inert filling material so that the gold nanoparticles were located at the central region of the rotor.

Reactions were monitored using Merck silica gel 60 F254 aluminum-backed plates. TLC plates were visualized by UV fluorescence ( $\lambda = 254$  and 365 nm) and  $\text{KMnO}_4$  stain. Flash column chromatography was performed using Sigma-Aldrich silica gel of 60–200  $\mu\text{m}$ .

Nanoparticle purification was performed by centrifugation using a Sigma high-speed centrifuge (3-30KS) equipped with a 12150-H rotor.<sup>12</sup>

High-resolution mass spectra were recorded on a micrOTOF-Bruker instrument with an ESI or APCI source.

UV/vis spectra were collected using an Agilent Cary 5000 UV–vis–NIR spectrometer using quartz cuvettes with a 10 mm path length. Samples were dissolved in  $\text{CH}_2\text{Cl}_2$ , toluene, or a mixture, as specified.

TEM samples were prepared by dropping colloidal suspensions onto a copper grid coated with a carbon film and allowing the solvent to evaporate in air. The TEM images were obtained using a Tecnai Spirit G2 microscope operating at 120 kV. Size distribution histograms were obtained by measuring at least 500 particles per sample using the ImageJ software.

XPS spectra were recorded with a Thermo ESCALAB 250Xi X-ray photoelectron spectrometer with a monochromatic Al-K $\alpha$  X-ray source ( $h\nu = 1486.6$  eV) operating at  $10^{-10}$  Torr. The analyzer pass energy was 100 eV for the survey spectra and 20 eV for the high-resolution spectra. All spectra were calibrated versus the binding energy (BE) of hydrocarbons (C 1s at 285.0 eV). The spectra were recorded and analyzed using the Thermo Advantage software. For curve fitting and decomposition, a Shirley-type background subtraction has been used, and the shape of the fitting curves was obtained by a 70% Gaussian/30% Lorentzian distribution.

**4.2. Synthesis of Precursors.** 1-Azidododecane,<sup>30</sup> 1-azidohexane,<sup>31</sup> and benzyl azide<sup>32</sup> were prepared following the reported procedures. Their spectroscopic data match those previously reported.<sup>30–32</sup>

**4.3. Synthesis of 1,2,3-Triazoles (1).** A round-bottom flask was charged with a stir bar, azide (1.0 equiv), alkyne (1.1 equiv),  $\text{CH}_2\text{Cl}_2$ /water (1.33:1; final reaction concentration, 0.33 M), and finally  $\text{CuSO}_4 \cdot 5\text{H}_2\text{O}$  (15 mol %). Sodium ascorbate (0.5 equiv) was then added to the vigorously stirred reaction portionwise. The reaction mixture was stirred overnight at room temperature and then quenched with conc.  $\text{NH}_4\text{OH}$  solution (~25% in water) to complex copper in the reaction mixture. The phases were then separated, and the aqueous phase was extracted with  $\text{CH}_2\text{Cl}_2$  (3 $\times$ ). Residual copper was removed by washing the combined organic phases with an aqueous EDTA solution (~0.02 M) until washes are clear (at least three times). The combined organic phases were then finally washed with brine and dried over anhydrous  $\text{MgSO}_4$ , filtered, and concentrated under reduced pressure onto Celite. The residue was purified by silica gel flash column chromatography using  $\text{CH}_2\text{Cl}_2$  (100%) to  $\text{CH}_2\text{Cl}_2$ /MeOH (95:5). Removal of the solvent under reduced pressure provided the product as a powder. Detailed

procedures for compounds **1a**, **1b**, **1c**, **1d**, and **1e**, along with their characterizations, are reported in the Supporting Information.

**4.4. Synthesis of 1,2,3-Triazolium Bromide Salts (2).** A pressure vial was charged with a stir bar, triazole **1** (1.0 equiv), alkyl bromide (10–20 equiv), and MeCN (0.2 M). The vial was sealed and stirred at 85  $^\circ\text{C}$  for the indicated time until the conversion is complete, as determined by  $^1\text{H}$  NMR spectroscopy. After cooling to room temperature, the reaction mixture was washed with petroleum ether (3 $\times$ ) to remove excess alkyl bromide. In the case of benzyl bromide, after washing with petroleum ether, the MeCN fraction was stirred with  $\text{NEt}_3$  (2.0 equiv relative to alkyl bromide) to remove traces of benzyl bromide. The MeCN fraction was then concentrated, and the residue was dissolved in  $\text{CH}_2\text{Cl}_2$ . The organic phase was washed with water (3 $\times$ ), then with brine (1 $\times$ ), then dried over anhydrous  $\text{MgSO}_4$ , filtered, and concentrated under reduced pressure. The residue was dissolved in a minimum of  $\text{CH}_2\text{Cl}_2$  and then dropped onto excess pentane; the mixture was sonicated and then placed into a  $-18$   $^\circ\text{C}$  freezer overnight for the precipitation of the product as a powder or oil. The supernatant was decanted, and the powder or oil was dried under high vacuum. Detailed procedures for compounds **2a** to **2g**, along with their characterizations, are reported in the Supporting Information. The synthesis of  $^{13}\text{C}$ -labeled **2a** (**2a\***), using  $^{13}\text{CBr}_4$  as the  $^{13}\text{C}$  source, is fully described in the Supporting Information with its spectroscopic characterization.

**4.5. Synthesis of 1,2,3-Triazolium Hexafluorophosphate Salts (2-PF<sub>6</sub>).** A round-bottom flask was charged with a stir bar, triazolium bromide salt **2** (1.0 equiv), and  $\text{CH}_2\text{Cl}_2$  (0.1 M).  $\text{KPF}_6$  (2.0 equiv) was added to the stirring reaction mixture and left to stir overnight at room temperature. The reaction mixture was then transferred to a separatory funnel and washed with water (2 $\times$ ) and brine (1 $\times$ ). The organic phase was dried over anhydrous  $\text{MgSO}_4$ , filtered, and concentrated under reduced pressure. The residue was dissolved in a minimum of  $\text{CH}_2\text{Cl}_2$  and then dropped onto excess pentane; the mixture was sonicated and then placed into a  $-18$   $^\circ\text{C}$  freezer overnight for the precipitation of the product as a powder or oil. The supernatant was decanted, and the powder or oil was dried under high vacuum. Detailed procedures for compounds **2a-PF<sub>6</sub>** and **2h-PF<sub>6</sub>**, along with their characterizations, are reported in the Supporting Information.

**4.6. Synthesis of MIC-Au(I) Chloride Complex 3a.** Adapting a described protocol,<sup>27a</sup> under Ar, a 100 mL round-bottom flask was charged with a stir bar, triazolium salt **2a** (1.25 g, 2.16 mmol),  $\text{CH}_2\text{Cl}_2$  (10 mL), and MeCN (10 mL). To the stirring reaction mixture,  $\text{Ag}_2\text{O}$  (0.58 equiv, 293.3 mg, 1.25 mmol) and  $\text{NMe}_4\text{Cl}$  (1.3 equiv, 314 mg, 2.81 mmol) were added, and the suspension was stirred for 16 h at room temperature, excluded from light, under an Ar atmosphere.  $\text{Me}_2\text{S} \bullet \text{AuCl}$  (1.1 equiv, 706.9 mg, 2.38 mmol) was then added, and the reaction mixture was stirred for an additional 2 h under Ar. The reaction mixture was then filtered over Celite, and the filtrate was concentrated under reduced pressure. The residue was resuspended in  $\text{CH}_2\text{Cl}_2$  and filtered over a three-layered plug of Celite–silica gel–Celite to remove insoluble salts and residues. The filtrate was then concentrated under reduced pressure to give the desired product as a white powder (1.6 g, >99%). Note: this complex tends to decompose on slight heating (40  $^\circ\text{C}$ ) to a light purple powder, indicating degradation to bulk Au(0). It is recommended to remove the solvent at room temperature under reduced pressure and to store the product at  $-18$   $^\circ\text{C}$ , protected from light. Spectroscopic details are reported in the Supporting Information.

**4.7. Synthesis of MIC-Au(III) Chloride Complex 3a'.** Adapting a described protocol,<sup>27b</sup> under Ar, a Schlenk flask was charged with **3a** (182 mg, 0.25 mmol),  $\text{PhICl}_2$  (1.5 equiv, 105 mg, 0.375 mmol), and dry  $\text{CH}_2\text{Cl}_2$  (6.5 mL). The flask was protected from light and stirred at room temperature for 18 h. The reaction mixture was then concentrated under reduced pressure, and pentane was added; the mixture was sonicated to produce a white precipitate. The heterogeneous mixture was loaded onto a silica gel plug, and the plug was washed with pentane; the product was then eluted with  $\text{CH}_2\text{Cl}_2$ . Removal of the solvent and drying under high vacuum

provided the desired product as a pale-yellow solid (202 mg, >99%). Spectroscopic details are reported in the Supporting Information.

**4.8. Synthesis of MIC-Coated Au Nanoparticles (MIC-AuNPs) from Triazolium Salts.** The following were weighed out in three separate vials: (1) triazolium salt **2** (0.14 mmol), (2) NaH (60% dispersion in mineral oil, 5.5 mg, 0.14 mmol), and (3)  $\text{HAuCl}_4 \cdot 3\text{H}_2\text{O}$  (13.5 mg, 0.03 mmol). The triazolium salt was dissolved in  $\text{CH}_2\text{Cl}_2$  (2 mL), and NaH was suspended in  $\text{CH}_2\text{Cl}_2$  (1 mL), and this suspension was added to the triazolium salt in solution (bubbling occurs); the NaH vial was rinsed with  $\text{CH}_2\text{Cl}_2$  (1 mL) and added to the triazolium salt/NaH reaction mixture. The triazolium salt/NaH mixture was stirred at room temperature for 5 min. In parallel,  $\text{HAuCl}_4 \cdot 3\text{H}_2\text{O}$  is dissolved into  $\text{CH}_2\text{Cl}_2$  (2 mL) (referred to as [Au] solution) with the aid of ultrasonication; after the triazolium salt/NaH mixture has been stirred for 5 min, the [Au] solution is added in one portion, the [Au] solution vial is rinsed with  $\text{CH}_2\text{Cl}_2$  ( $2 \times 1$  mL), and the washings are added to the reaction vial. A fresh aqueous  $\text{NaBH}_4$  (10 equiv, 13.2 mg, 0.34 mmol) solution was prepared by dissolving in water (2 mL). After the triazolium salt/NaH/[Au] mixture has been stirred for 5 min (900 rpm), the aq.  $\text{NaBH}_4$  solution is added in one portion using a syringe. This causes immediate gas evolution, and the reaction mixture turns from yellow/orange to deep burgundy red. The reaction vial was wrapped in an aluminum foil to protect the reaction from light, and the biphasic mixture was vigorously stirred (900 rpm) for 18 h at room temperature. The phases were allowed to separate, and the aqueous layer was removed using a pipette; the organic phase was washed with water ( $2 \times 5$  mL). The organic phase was then concentrated under a flow of argon to  $\sim 2$  mL. The organic phase was then divided ( $\sim 1$  mL/tube) into two centrifuge tubes (Thermo Scientific, Oak Ridge Centrifuge Nalgene Tube, PPCO, 3119-0050), and the MIC-AuNPs were precipitated with EtOH ( $\sim 50$  mL/tube). The tubes were centrifuged at 19,000 rpm (33,902 RCF) for 45 min. The supernatant was decanted, and the MIC-AuNPs pellets were resuspended in a minimum of  $\text{CH}_2\text{Cl}_2$  ( $\sim 1$  mL/tube) and reprecipitated with EtOH ( $\sim 50$  mL/tube) and centrifuged at 21,000 rpm (41,415 RCF) for 1 h. To increase the recovery of MIC-AuNPs from the EtOH supernatant, all volatiles can be removed under reduced pressure, and the residue is resuspended in a minimum of  $\text{CH}_2\text{Cl}_2$  ( $< 2$  mL), reprecipitated with EtOH, and collected by centrifugation. The supernatant was decanted, and the MIC-AuNPs were dissolved in a minimum of  $\text{CH}_2\text{Cl}_2$  for storage. For each MIC-AuNP batch prepared, its UV/vis spectrum, the representative TEM image, and its size distribution are given in the Supporting Information.

**4.9. Synthesis of MIC-Coated Au Nanoparticles (MIC-AuNPs) from MIC-AuCl (3a) or MIC-AuCl<sub>3</sub> (3a').** Example of the protocol using **3a**: the MIC-Au(I) chloride complex **3a** (25.0 mg, 0.03 mmol) was added to a vial and dissolved in  $\text{CH}_2\text{Cl}_2$  (8 mL). A fresh aqueous  $\text{NaBH}_4$  (10 equiv, 13.2 mg, 0.34 mmol) solution in water (2 mL) is directly added in one portion using a syringe to the stirring mixture (900 rpm). After 5 min of stirring, the reaction mixture turns from clear to deep burgundy red. The reaction vial is wrapped in an aluminum foil to protect the reaction from light, and the biphasic mixture is vigorously stirred (900 rpm) for 18 h at room temperature. The phases are allowed to separate; the aqueous layer is removed using a pipette, and the organic phase is washed with water ( $3 \times 5$  mL). The organic phase is then concentrated under a flow of argon to  $\sim 2$  mL. The organic phase is then divided ( $\sim 1$  mL/tube) into two centrifuge tubes (Thermo Scientific, Oak Ridge Centrifuge Nalgene Tube, PPCO, 3119-0050), and the MIC-AuNPs are precipitated with EtOH ( $\sim 50$  mL/tube). The tubes were centrifuged at 19,000 rpm (33,902 RCF) for 45 min. The supernatant was decanted, and the MIC-AuNPs pellets were suspended in a minimum of  $\text{CH}_2\text{Cl}_2$  ( $\sim 1$  mL/tube) and reprecipitated with EtOH ( $\sim 50$  mL/tube) and centrifuged at 21,000 rpm (41,415 RCF) for 1 h. To increase the recovery of MIC-AuNPs from the EtOH supernatant, all volatiles can be removed under reduced pressure and the residue resuspended in a minimum of  $\text{CH}_2\text{Cl}_2$  ( $< 2$  mL), reprecipitated with EtOH, and collected by centrifugation. The supernatant was decanted, and **3a-MIC-AuNP** was dissolved in a minimum of

$\text{CH}_2\text{Cl}_2$  or toluene for storage. The same protocol was followed for **3a'-MIC-AuNP**, replacing **3a** by **3a'**. The UV/vis spectra, the representative TEM picture, and size distribution are given in the Supporting Information for **3a-MIC-AuNP** and **3a'-MIC-AuNP**.

**4.10. Catalytic Reduction of 4-Nitrophenol (4-NP) Using MIC-AuNP at Room Temperature.** 4-Nitrophenol (0.35 mg, 2.5  $\mu\text{mol}$ ) was dissolved in 5 mL of ultrapure water. A large excess of  $\text{NaBH}_4$  (1000 equiv, 95 mg, 2.5 mmol), dissolved in 10 mL of ultrapure water, was added to the 4-nitrophenol solution. 3 mL of this mixture was transferred to a quartz cuvette to record its UV/vis spectrum, which did not show any evolution with time. This first UV/vis spectrum corresponds to  $t = 0$  s for the kinetics. Then, this 3 mL of the mixture was returned back to the mother solution and vigorously mixed. In another vial, 20  $\mu\text{L}$  of an MIC-AuNP suspension (from 1 to 0.6 mg/mL,  $\text{CH}_2\text{Cl}_2$ ) was diluted to 2 mL with  $\text{CH}_2\text{Cl}_2$ . This 2 mL of diluted MIC-AuNP suspension (from 0.01 to 0.006 mg/mL) was rapidly added to the 4-nitrophenol aqueous solution under stirring. At different times, the stirring was stopped, and, once the two phases were separated, 3 mL of the top aqueous layer was taken to record its UV/vis spectrum. Then, the 3 mL was returned back to the main reaction vessel and stirred again till the next time point. The reaction was monitored until the yellow color of the aqueous phase had disappeared, signifying the endpoint of the reaction.

## ■ ASSOCIATED CONTENT

### SI Supporting Information

The Supporting Information is available free of charge at <https://pubs.acs.org/doi/10.1021/acs.chemmater.3c01162>.

Detailed synthetic protocols, characterization data (NMR and HRMS) for all synthesized compounds, characterization data (UV/vis and TEM) for all prepared AuNPs, additional XPS data,  $^1\text{H}$  and  $^{13}\text{C}$  solution NMR spectra of MIC-AuNP suspensions,  $^{13}\text{C}$  CP/MAS NMR of MIC-AuNPs, and catalysis data (PDF)

## ■ AUTHOR INFORMATION

### Corresponding Authors

Louis Fensterbank – Sorbonne Université, CNRS, Institut Parisien de Chimie Moléculaire (IPCM), F-75252 Paris Cedex 05, France; [orcid.org/0000-0003-0001-7120](https://orcid.org/0000-0003-0001-7120); Email: [louis.fensterbank@sorbonne-universite.fr](mailto:louis.fensterbank@sorbonne-universite.fr)

François Ribot – Sorbonne Université, CNRS, Laboratoire de Chimie de la Matière Condensée de Paris (LCMCP), F-75252 Paris Cedex 05, France; [orcid.org/0000-0001-5576-7725](https://orcid.org/0000-0001-5576-7725); Email: [francois.ribot@sorbonne-universite.fr](mailto:francois.ribot@sorbonne-universite.fr)

### Authors

Alexandre Porcheron – Sorbonne Université, CNRS, Laboratoire de Chimie de la Matière Condensée de Paris (LCMCP), F-75252 Paris Cedex 05, France; Sorbonne Université, CNRS, Institut Parisien de Chimie Moléculaire (IPCM), F-75252 Paris Cedex 05, France

Omar Sadek – Sorbonne Université, CNRS, Institut Parisien de Chimie Moléculaire (IPCM), F-75252 Paris Cedex 05, France; Present Address: Université Paris-Saclay, CNRS, Institut de Chimie Moléculaire et des Matériaux d'Orsay (ICMMO), F-91400 Orsay Cedex, France; [orcid.org/0000-0003-1853-541X](https://orcid.org/0000-0003-1853-541X)

Salem Ba Sowid – Sorbonne Université, CNRS, Laboratoire de Chimie de la Matière Condensée de Paris (LCMCP), F-75252 Paris Cedex 05, France; Sorbonne Université, CNRS, Institut Parisien de Chimie Moléculaire (IPCM), F-75252 Paris Cedex 05, France

**Nathalie Bridonneau** – Sorbonne Université, CNRS, Laboratoire de Chimie de la Matière Condensée de Paris (LCMCP), F-75252 Paris Cedex 05, France; Present Address: Université Paris-Saclay, CNRS, Institut de Chimie Moléculaire et des Matériaux d'Orsay (ICMMO), F-91400 Orsay Cedex, France

**Laura Hippolyte** – Sorbonne Université, CNRS, Laboratoire de Chimie de la Matière Condensée de Paris (LCMCP), F-75252 Paris Cedex 05, France; Sorbonne Université, CNRS, Institut Parisien de Chimie Moléculaire (IPCM), F-75252 Paris Cedex 05, France

**Dimitri Mercier** – PSL Research University, CNRS, Chimie ParisTech, Institut de Recherche de Chimie Paris (IRCP), Physical Chemistry of Surfaces Research Group, F-75005 Paris, France

**Philippe Marcus** – PSL Research University, CNRS, Chimie ParisTech, Institut de Recherche de Chimie Paris (IRCP), Physical Chemistry of Surfaces Research Group, F-75005 Paris, France; [orcid.org/0000-0002-9140-0047](https://orcid.org/0000-0002-9140-0047)

**Lukmonjon Mutalliev** – Sorbonne Université, CNRS, Institut Parisien de Chimie Moléculaire (IPCM), F-75252 Paris Cedex 05, France

**Clément Chauvier** – Sorbonne Université, CNRS, Institut Parisien de Chimie Moléculaire (IPCM), F-75252 Paris Cedex 05, France; [orcid.org/0000-0002-3782-8130](https://orcid.org/0000-0002-3782-8130)

**Corinne Chanéac** – Sorbonne Université, CNRS, Laboratoire de Chimie de la Matière Condensée de Paris (LCMCP), F-75252 Paris Cedex 05, France; [orcid.org/0000-0001-9785-1052](https://orcid.org/0000-0001-9785-1052)

Complete contact information is available at:

<https://pubs.acs.org/10.1021/acs.chemmater.3c01162>

## Author Contributions

The manuscript was written through contributions of all authors. All authors have given approval to the final version of the manuscript. A.P., O.S., and S.B.S. contributed equally.

## Funding

Initiative pour les Sciences et l'Ingénierie Moléculaire de l'Alliance Sorbonne Université; Agence Nationale pour la Recherche (ANR).

## Notes

The authors declare no competing financial interest.

## ACKNOWLEDGMENTS

The authors acknowledge Sorbonne Université, CNRS, and IUF for financial support and the SM3 platform of SU for high-resolution mass spectrometry analysis. This work has been supported by the Initiative pour les Sciences et l'Ingénierie Moléculaires de l'Alliance Sorbonne Université (SU), in the frame of the project MIC-Au, and the Agence Nationale de la Recherche (ANR), in the frame of the project COCOsMEN (ANR-18-CE09-0002). L.M. gratefully acknowledges "El-Yurt Umidi" Foundation for his PhD grant.

## REFERENCES

(1) (a) *Nanoparticles: From Theory to Application*; Schmid, G., Ed.; Wiley-VCH, 2010. (b) Stark, W. J.; Stoessel, P. R.; Wohlleben, W.; Hafner, A. Industrial Applications of Nanoparticles. *Chem. Soc. Rev.* **2015**, *44*, 5793–5805. (c) Mitchell, M. J.; Billingsley, M. M.; Haley, R. M.; Wechsler, M. E.; Peppas, N. A.; Langer, R. Engineering Precision Nanoparticles for Drug Delivery. *Nat. Rev. Drug Discovery* **2021**, *20*, 101–124.

(2) *Gold Nanoparticles for Physics, Chemistry and Biology*, 2nd ed.; Louis, C.; Pluchery, O., Eds.; World Scientific, 2017.

(3) (a) Her, S.; Jaffray, D. A.; Allen, C. Gold Nanoparticles for Applications in Cancer Radiotherapy: Mechanisms and Recent Advancements. *Adv. Drug Delivery Rev.* **2017**, *109*, 84–101. (b) Zeng, S.; Yong, K.-T.; Roy, I.; Dinh, X.-Q.; Yu, X.; Luan, F. A Review on Functionalized Gold Nanoparticles for Biosensing Applications. *Plasmonics* **2011**, *6*, 491–506. (c) Dreaden, E. C.; Alkilany, A. M.; Huang, X.; Murphy, C. J.; El-Sayed, M. A. The Golden Age: Gold Nanoparticles for Biomedicine. *Chem. Soc. Rev.* **2012**, *41*, 2740–2779. (d) Daniel, M. C.; Astruc, D. Gold Nanoparticles: Assembly, Supramolecular Chemistry, Quantum-Size-Related Properties, and Applications Toward Biology, Catalysis, and Nanotechnology. *Chem. Rev.* **2004**, *104*, 293–346.

(4) (a) Zhukhovitskiy, A. V.; MacLeod, M. J.; Johnson, J. A. Carbene Ligands in Surface Chemistry: From Stabilization of Discrete Elemental Allotropes to Modification of Nanoscale and Bulk Substrates. *Chem. Rev.* **2015**, *115*, 11503–11532. (b) Smith, C. A.; Narouz, M. R.; Lumis, P. A.; Singh, I.; Nazemi, A.; Li, C.-H.; Crudden, C. M. N-Heterocyclic Carbenes in Materials Chemistry. *Chem. Rev.* **2019**, *119*, 4986–5056. (c) An, Y.; Yu, J.; Han, Y. Recent Advances in the Chemistry of N-Heterocyclic-Carbene-Functionalized Metal-Nanoparticles and Their Applications. *Chin. J. Chem.* **2019**, *37*, 76–87. (d) Ranganath, K. V. S.; Kloesges, J.; Schäffer, A. H.; Glorius, F. Asymmetric Nanocatalysis: N-Heterocyclic Carbenes as Chiral Modifiers of Fe<sub>3</sub>O<sub>4</sub>/Pd nanoparticles. *Angew. Chem., Int. Ed.* **2010**, *49*, 7786–7789. (e) Richter, C.; Schaepe, K.; Glorius, F.; Jan Ravoo, B. Tailor-Made N-Heterocyclic Carbenes for Nanoparticle Stabilization. *Chem. Commun.* **2014**, *50*, 3204–3207. (f) Rühling, A.; Schaepe, K.; Rakers, L.; Vonhören, B.; Tegeder, P.; Ravoo, B. J.; Glorius, F. Modular Bidentate Hybrid NHC-Thioether Ligands for the Stabilization of Palladium Nanoparticles in Various Solvents. *Angew. Chem., Int. Ed.* **2016**, *55*, 5856–5860. (g) Wang, G.; Rühling, A.; Amirjalayer, S.; Knor, M.; Ernst, J. B.; Richter, C.; Gao, H. J.; Timmer, A.; Gao, H. Y.; Doltsinis, N. L.; Glorius, F.; Fuchs, H. Ballbot-Type Motion of N-Heterocyclic Carbenes on Gold Surfaces. *Nat. Chem.* **2017**, *9*, 152–156. (h) Nguyen, D. T.; Freitag, M.; Gutheil, C.; Sothewes, K.; Tyler, B. J.; Böckmann, M.; Das, M.; Schlüter, F.; Doltsinis, N. L.; Arlinghaus, H. F.; Ravoo, B. J.; Glorius, F. An Arylazopyrazole-Based N-Heterocyclic Carbene as a Photo-switch on Gold Surfaces: Light-Switchable Wettability, Work Function, and Conductance. *Angew. Chem., Int. Ed.* **2020**, *59*, 13651–13656. (i) Koy, M.; Bellotti, P.; Das, M.; Glorius, F. N-Heterocyclic Carbenes as Tunable Ligands for Catalytic Metal Surfaces. *Nat. Catal.* **2021**, *4*, 352–363.

(5) (a) Crudden, C. M.; Horton, J. H.; Ebralidze, I. I.; Zenkina, O. V.; McLean, A. B.; Drevniok, B.; She, Z.; Kraatz, H.; Mosey, N. J.; Seki, T.; Keske, E. C.; Leake, J. D.; Rousina-Webb, A.; Wu, G. Ultra-Stable Self-Assembled Mono-layers of N-Heterocyclic Carbenes on Gold. *Nat. Chem.* **2014**, *6*, 409–414. (b) Sherman, L. M.; Strausser, S. L.; Borsari, R. K.; Jenkins, D. M.; Camden, J. P. Imidazolium N-Heterocyclic Carbene Ligands for Enhanced Stability on Gold Surfaces. *Langmuir* **2021**, *37*, 5864–5871.

(6) Bakker, A.; Freitag, M.; Kolodzeiski, E.; Bellotti, P.; Timmer, A.; Ren, J.; Schulze Lammers, B.; Moock, D.; Roesky, H. W.; Mönig, H.; Amirjalayer, S.; Fuchs, H.; Glorius, F. An Electron-Rich Cyclic (Alkyl)(Amino)Carbene on Au(111), Ag(111), and Cu(111) Surfaces. *Angew. Chem., Int. Ed.* **2020**, *59*, 13643–13646.

(7) (a) Hopkinson, M. N.; Richter, C.; Schedler, M.; Glorius, F. An Overview of N-Heterocyclic Carbenes. *Nature* **2014**, *510*, 485–496. (b) Huynh, H. V. Electronic Properties of N-Heterocyclic Carbenes and Their Experimental Determination. *Chem. Rev.* **2018**, *118*, 9457–9492.

(8) Hurst, E. C.; Wilson, K.; Fairlamb, I. J. S.; Chechik, V. N-Heterocyclic Carbene Coated Metal Nanoparticles. *New J. Chem.* **2009**, *33*, 1837–1840.

(9) Vignolle, J.; Tilley, T. D. N-Heterocyclic Carbene-Stabilized Gold Nanoparticles and Their Assembly into 3D Superlattices. *Chem. Commun.* **2009**, *46*, 7230–7232.

- (10) For recent and leading references, see: (a) Serpell, C. J.; Cookson, J.; Thompson, A. L.; Brown, C. M.; Beer, P. D. Haloaurate and Halopalladate Imidazolium Salts: Structures, Properties, and Use as Precursors for Catalytic Metal Nanoparticles. *Dalton Trans.* **2013**, 42, 1385–1393. (b) Crespo, J.; Guari, Y.; Ibarra, A.; Larionova, J.; Lasanta, T.; Laurencin, D.; López-de-Luzuriaga, J. M.; Monge, M.; Olmos, M. E.; Richeter, S. Ultrasmall NHC-Coated Gold Nanoparticles Obtained through Solvent Free Thermolysis of Organometallic Au(I) Complexes. *Dalton Trans.* **2014**, 43, 15713–15718. (c) Ferry, A.; Schaepe, K.; Tegeder, P.; Richter, C.; Chepiga, K. M.; Ravoo, B. J.; Glorius, F. Negatively Charged N-Heterocyclic Carbene-Stabilized Pd and Au Nanoparticles and Efficient Catalysis in Water. *ACS Catal.* **2015**, 5, 5414–5420. (d) MacLeod, M. J.; Johnson, J. A. PEGylated N-Heterocyclic Carbene Anchors Designed to Stabilize Gold Nanoparticles in Biologically Relevant Media. *J. Am. Chem. Soc.* **2015**, 137, 7974–7977. (e) Narouz, M. R.; Li, C.-H.; Nazemi, A.; Crudden, C. M. Amphiphilic N-Heterocyclic Carbene-Stabilized Gold Nanoparticles and Their Self-Assembly in Polar Solvents. *Langmuir* **2017**, 33, 14211–14219. (f) Salorinne, K.; Man, R. W. Y.; Li, C.-H.; Taki, M.; Nambo, M.; Crudden, C. M. Water-Soluble N-Heterocyclic Carbene-Protected Gold Nanoparticles: Size-Controlled Synthesis, Stability, and Optical Properties. *Angew. Chem., Int. Ed.* **2017**, 56, 6198–6202. (g) Young, A. J.; Sauer, M.; Rubio, G. M. D. M.; Sato, A.; Foelske, A.; Serpell, C. J.; Chin, J. M.; Reithofer, M. R. One-Step Synthesis and XPS Investigations of Chiral NHC–Au(0)/Au(I) Nanoparticles. *Nanoscale* **2019**, 11, 8327–8333. (h) Nosratabad, N. A.; Jin, Z.; Du, L.; Thakur, M.; Mattoussi, H. N-Heterocyclic Carbene-Stabilized Gold Nanoparticles: Mono- Versus Multidentate Ligands. *Chem. Mater.* **2021**, 33, 921–933.
- (11) Rúbio, G. M. D. M.; Keppler, B. K.; Chin, J. M.; Reithofer, M. R. Synthetically Versatile Nitrogen Acyclic Carbene Stabilized Gold Nanoparticles. *Chem. – A Eur. J.* **2020**, 26, 15859–15862.
- (12) (a) Rostovtsev, V. V.; Green, L. G.; Fokin, V. V.; Sharpless, K. B. A Stepwise Huisgen Cycloaddition Process: Copper(I)-Catalyzed Regioselective “Ligation” of Azides and Terminal Alkynes. *Angew. Chem., Int. Ed.* **2002**, 41, 2596–2599. (b) Tornøe, C. W.; Christensen, C.; Meldal, M. Peptidotriazoles on solid phase: [1,2,3]-triazoles by regioselective copper(i)-catalyzed 1,3-dipolar cycloadditions of terminal alkynes to azides. *J. Org. Chem.* **2002**, 67, 3057–3064.
- (13) Albrecht, M. Abnormal Carbenes as Ligands in Transition Metal Chemistry: Curiosities with Exciting Perspectives. *Chimia* **2009**, 63, 105–110.
- (14) Guisado-Barríos, G.; Soleilhavoup, M.; Bertrand, G. 1 H-1,2,3-Triazol-5-Ylidenes: Readily Available Mesoionic Carbenes. *Acc. Chem. Res.* **2018**, 51, 3236–3244.
- (15) (a) Nguyen, D. T. H.; Bélanger-Bouliga, M.; Shultz, L. R.; Maity, A.; Jurca, T.; Nazemi, A. Robust Water-Soluble Gold Nanoparticles via Polymerized Mesoionic N-Heterocyclic Carbene–Gold(I) Complexes. *Chem. Mater.* **2021**, 33, 9588–9600. (b) Cui, L.; Du, M.; Guo, S. Preparation, Characterization and Stability Studies of Gold Nanoparticles Capped by 1,2,3-Triazole-Based Mesoionic Carbenes. *ChemistrySelect* **2022**, 7, No. e202201999.
- (16) (a) Hippolyte, L. New syntheses of N-heterocyclic carbene-stabilized gold nanoparticles. Ph.D. Dissertation, Sorbonne Université, Paris, France, 2018, <https://theses.hal.science/tel-03029247>. (b) Porcheron, A. Plasmonic nanoparticles modified by coordination complexes. Ph.D. Dissertation, Sorbonne Université: Paris, France, 2021, <https://www.theses.fr/2021SORUS471>. (c) Porcheron, A.; Sadek, O.; Ba Sowid, S.; Bridonneau, N.; Hippolyte, L.; Mercier, D.; Marcus, P.; Chauvier, C.; Chanéac, C.; Fensterbank, L.; Ribot, F. Direct Synthesis of Mesoionic Carbene (MIC) Stabilized Gold Nanoparticles from 1,2,3-Triazolium Salts. *ChemRxiv.* **2022**, DOI: 10.26434/chemrxiv-2022-krbwv-v2.
- (17) Bridonneau, N.; Hippolyte, L.; Mercier, D.; Portehault, D.; Desage-El Murr, M.; Marcus, P.; Fensterbank, L.; Chanéac, C.; Ribot, F. N-Heterocyclic Carbene-Stabilized Gold Nanoparticles with Tunable Sizes. *Dalton Trans.* **2018**, 47, 6850–6859.
- (18) (a) Pellas, V.; Hu, D.; Mazouzi, Y.; Mimoun, Y.; Blanchard, J.; Guibert, C.; Salmain, M.; Boujday, S. Gold Nanorods for LSPR Biosensing: Synthesis, Coating by Silica, and Bioanalytical Applications. *Biosensors* **2020**, 10, 146. (b) Booth, S. G.; Uehara, A.; Chang, S.-Y.; La Fontaine, C.; Fujii, T.; Okamoto, Y.; Imai, T.; Schroeder, S. L. M.; Dryfe, R. A. W. The significance of bromide in the Brust–Schiffrin synthesis of thiol protected gold nanoparticles. *Chem. Sci.* **2017**, 8, 7954–7962.
- (19) (a) Lara, P.; Rivada-Wheelaghan, O.; Conejero, S.; Poteau, R.; Philippot, K.; Chaudret, B. Ruthenium Nanoparticles Stabilized by N-Heterocyclic Carbenes: Ligand Location and Influence on Reactivity. *Angew. Chem., Int. Ed.* **2011**, 50, 12080–12084. (b) Goldmann, C.; Ribot, F.; Peiretti, L. F.; Quaino, P.; Tielens, F.; Sanchez, C.; Chanéac, C.; Portehault, D. Quantified Binding Scale of Competing Ligands at the Surface of Gold Nanoparticles: The Role of Entropy and Intermolecular Forces. *Small* **2017**, 13, No. 1604028.
- (20) The presence of molecular species can be easily observed in insufficiently purified samples, or in the supernatant following MIC–AuNPs purification by centrifugation, see [Figures S28–S31](#).
- (21) Narouz, M. R.; Takano, S.; Lummis, P. A.; Levchenko, T. I.; Nazemi, A.; Kaappa, S.; Malola, S.; Yousefzaladeh, G.; Calhoun, L. A.; Stampelcoskie, K. G.; Häkkinen, H.; Tsukuda, T.; Crudden, C. M. Robust, Highly Luminescent Au<sub>13</sub> Superatoms Protected by N-Heterocyclic Carbenes. *J. Am. Chem. Soc.* **2019**, 141, 14997–15002.
- (22) Weinberger, D. S.; Melaimi, M.; Moore, C. E.; Rheingold, A. L.; Frenking, G.; Jerabek, P.; Bertrand, G. Isolation of Neutral Mono- and Dinuclear Gold Complexes of Cyclic(Alkyl)(amino)carbenes. *Angew. Chem., Int. Ed.* **2013**, 52, 8964–8967.
- (23) Kaeffer, N.; Mance, D.; Copéret, C. N-Heterocyclic Carbene Coordination to Surface Copper Sites in Selective Semihydrogenation Catalysts from Solid-State NMR Spectroscopy. *Angew. Chem., Int. Ed.* **2020**, 59, 19999–20007.
- (24) An important experimental factor we observed that merits mention is that the counter ion plays a key role in the stability of the triazolium salt precursor under X-ray irradiation. During experiments an evolution of the N 1s signal is observed with the emergence of a new component at a lower binding energy. This effect was significant for **2a** while only trace modifications to spectra were observed using **2h-PF<sub>6</sub>** (see [Figure S16](#)).
- (25) Morel, A.-L.; Volmant, R.-M.; Méthivier, C.; Krafft, J.-M.; Boujday, S.; Pradier, C.-M. Optimized Immobilization of Gold Nanoparticles on Planar Surfaces through Alkylthiols and Their Use to Build 3D Biosensors. *Colloids Surf., B* **2010**, 81, 304–312.
- (26) Man, R. W. Y.; Li, C.-H.; MacLean, M. W. A.; Zenkina, O. V.; Zamora, M. T.; Saunders, L. N.; Rousina-Webb, A.; Nambo, M.; Crudden, C. M. Ultraprecise Gold Nanoparticles Modified by Bidentate N-Heterocyclic Carbene Ligands. *J. Am. Chem. Soc.* **2018**, 140, 1576–1579.
- (27) (a) Pretorius, R.; Fructos, M. R.; Müller-Bunz, H.; Gossage, R. A.; Pérez, P. J.; Albrecht, M. Synthesis and Catalytic Applications of 1,2,3-Triazolylidene Gold(I) Complexes in Silver-Free Oxazoline Syntheses and C–H Bond Activation. *Dalton Trans.* **2016**, 45, 14591–14602. (b) Navarro, M.; Tabey, A.; Szalóki, G.; Mallet-Ladeira, S.; Bourissou, D. Stable Au(III) Complexes Bearing Hemilabile P<sup>N</sup> and C<sup>N</sup> Ligands: Coordination of the Pendant Nitrogen upon Oxidation of Gold. *Organometallics* **2021**, 40, 1571–1576.
- (28) Aditya, T.; Pal, A.; Pal, T. Nitroarene reduction: a trusted model reaction to test nanoparticle catalysts. *Chem. Commun.* **2015**, 51, 9410–9431.
- (29) (a) Wen, X.; Li, G.; Chen, Q.; Zhang, H.; Ba, X.; Bai, G. Organic-Soluble Palladium Nanoparticles Costabilized by Hyperbranched Polymer and Dispersants as Highly Efficient and Reusable Catalysts in Biphasic Solution. *Ind. Eng. Chem. Res.* **2014**, 53, 11646–11652. (b) Liu, F.; Liu, X.; Astruc, D.; Gu, H. Dendronized Triazolyl-Containing Ferrocenyl Polymers as Stabilizers of Gold Nanoparticles for Recyclable Two-Phase Reduction of 4-Nitrophenol. *J. Colloid Interface Sci.* **2019**, 533, 161–170.

(30) Sayed, S. Y.; Bayat, A.; Kondratenko, M.; Leroux, Y.; Hapiot, P.; McCreery, R. L. Bilayer Molecular Electronics: All-Carbon Electronic Junctions Containing Molecular Bilayers Made with “Click” Chemistry. *J. Am. Chem. Soc.* **2013**, *135*, 12972–12975.

(31) Sinha, J.; Sahoo, R.; Kumar, A. Processable, Regioregular, and “Click”able Monomer and Polymers Based on 3,4-Propylenedioxythiophene with Tunable Solubility. *Macromolecules* **2009**, *42*, 2015–2022.

(32) Berry, M. T.; Castrejon, D.; Hein, J. E. Oxidative Esterification of Aldehydes Using Mesoionic 1,2,3-Triazolyl Carbene Organo-catalysts. *Org. Lett.* **2014**, *16*, 3676–3679.